The Increasing Efficiency of the Poleward Energy Transport into the Arctic in a Warming Climate

Christopher J. Cardinale[1] and Brian E. J. Rose[2]

[1]University at Albany, State University of New York
[2]University at Albany

November 24, 2022

Abstract

This study quantifies the contribution to Arctic winter surface warming from changes in the tropospheric energy transport (F_{trop}) and the efficiency with which F_{trop} heats the surface in the RCP8.5 warming scenario of the CESM Large Ensemble. A metric for this efficiency, E_{trop}, measures the fraction of anomalous F_{trop} that is balanced by an anomalous net surface flux (NSF). Drivers of E_{trop} are identified in synoptic-scale events during which F_{trop} is the dominant driver of NSF. E_{trop} is sensitive to the vertical structure of F_{trop} and pre-existing Arctic lower-tropospheric stability (LTS). In RCP8.5, winter mean F_{trop} decreases by 9.5 Wm^{-2}, while E_{trop} increases by 5.7%, likely driven by decreased Arctic LTS, indicating an increased coupling between F_{trop} and the surface energy budget. The net impact of decreasing F_{trop} and increasing efficiency is a positive 0.7 Wm^{-2} contribution to winter-season surface heating.

The Increasing Efficiency of the Poleward Energy Transport into the Arctic in a Warming Climate

Christopher J. Cardinale[1], and Brian E. J. Rose[1]

[1]Department of Atmospheric and Environmental Sciences, University at Albany, State University of New York, Albany, New York

Key Points:

- The poleward atmospheric energy flux into the Arctic decreases in the RCP8.5 warming scenario of the CESM Large Ensemble
- The efficiency with which the atmospheric energy flux heats the Arctic surface increases in the RCP8.5 warming scenario
- Changes in the atmospheric energy flux contribute to Arctic surface warming despite a decrease in the vertical integral of the energy flux

Corresponding author: Christopher J. Cardinale, ccardinale@albany.edu

Abstract

This study quantifies the contribution to Arctic winter surface warming from changes in the tropospheric energy transport (F_{trop}) and the efficiency with which F_{trop} heats the surface in the RCP8.5 warming scenario of the CESM Large Ensemble. A metric for this efficiency, E_{trop}, measures the fraction of anomalous F_{trop} that is balanced by an anomalous net surface flux (NSF). Drivers of E_{trop} are identified in synoptic-scale events during which F_{trop} is the dominant driver of NSF. E_{trop} is sensitive to the vertical structure of F_{trop} and pre-existing Arctic lower-tropospheric stability (LTS). In RCP8.5, winter mean F_{trop} decreases by 9.5 W m^{-2}, while E_{trop} increases by 5.7%, likely driven by decreased Arctic LTS, indicating an increased coupling between F_{trop} and the surface energy budget. The net impact of decreasing F_{trop} and increasing efficiency is a positive 0.7 W m^{-2} contribution to winter-season surface heating.

Plain Language Summary

The role of atmospheric circulations in future Arctic surface warming is typically assessed through changes in total energy transported into the Arctic, assuming a vertically uniform temperature response. However, the Arctic response to energy input during short timescale winter weather events is sensitive to the vertical structure of the transport and the pre-existing surface state. Using climate model simulations with increasing greenhouse gases, this study quantifies changes in the fraction of excess energy absorbed by the surface during individual weather events. The total energy transport is found to decrease. However, this decrease is overcompensated by an increase in the per-event surface heating efficiency. The net effect is a small positive contribution to Arctic surface warming.

1 Introduction

Bottom-amplified warming of the Arctic is consistently found in recent observations (Screen & Simmonds, 2010; Cohen et al., 2014) and climate model projections (Boeke & Taylor, 2018), with surface air temperatures increasing at a faster rate than the global average, especially during the cold season. However, models disagree on the change in atmospheric energy transport, and the role of atmospheric circulations in Arctic warming is still debated (e.g., Taylor et al., 2022).

A frequently-used metric of the influence of atmospheric circulations on Arctic surface climate is F_{wall}, the total vertically- and zonally-integrated moist static energy (MSE) flux into the polar cap (or equivalently, the total cap-averaged MSE flux convergence) (e.g., Hwang et al., 2011; Koenigk et al., 2013; Pithan & Mauritsen, 2014; Goosse et al., 2018; Boeke & Taylor, 2018; Feldl et al., 2020; Hahn et al., 2021). Previous attribution studies have found relatively small impacts of F_{wall} changes on Arctic warming and amplification (e.g., Pithan & Mauritsen, 2014; Feldl et al., 2020; Hahn et al., 2021). F_{wall} changes are anti-correlated with Arctic amplification across models and are thus inferred to dampen inter-model spread of amplification (Boeke & Taylor, 2018). However, as we review below, F_{wall} is a limited metric that may not fully capture the causal effects of atmospheric motions on Arctic surface warming. The goal of this study is to apply an improved metric to a climate change scenario in a comprehensive model to assess whether atmospheric circulations dampen or amplify Arctic surface warming.

One difficulty with the interpretation of F_{wall} is its non-negligible stratospheric contribution. Cardinale et al. (2021) found that 19% of winter-mean MSE flux occurs above 300 hPa and has little influence on the Arctic surface energy budget. They also showed that the integrated *tropospheric* MSE flux below 300 hPa (F_{trop}) is better correlated with near-surface air temperature variability on daily to monthly time scales. This is our main motivation for focusing strictly on F_{trop} in this work.

Another limitation of F_{wall} is that not all energy flux events have equivalent impact on the surface. MSE flux is often partitioned into latent heat (LH) and dry static energy (DSE; the sum of sensible heat and geopotential) flux components (e.g., Koenigk et al., 2013; Feldl et al., 2020; Hahn et al., 2021). LH has an amplified warming effect on the Arctic due to its relationship with cloud and atmospheric emissivity changes (Graversen & Burtu, 2016; Baggett & Lee, 2017; Graversen & Langen, 2019). The DSE component of F_{wall} tends to decrease in a warmer climate, compensated by an increase in LH (e.g., Hwang et al., 2011; Koenigk et al., 2013; Graversen & Burtu, 2016; Hahn et al., 2021). However, attribution studies typically do not consider the amplified warming effect of increased LH and contributions from energy transport changes to lapse-rate changes (Henry et al., 2021). The degree of compensation between LH and DSE components is sensitive to the definition of the Arctic cap and on the magnitude of Arctic amplification (Boeke & Taylor, 2018); more models show a decrease in F_{wall} when defined at 70°N rather than 60°N (Hwang et al., 2011).

Recent work has focused attention on the climatic impact of synoptic-timescale variability of poleward fluxes. Episodic F_{trop} events—commonly referred to as moist intrusions—are events of poleward F_{trop} anomalies that temporarily warm the Arctic and reduce sea ice growth through increased downward longwave radiation and reduced upward turbulent heat fluxes (e.g., Doyle et al., 2011; Woods et al., 2013; D.-S. R. Park et al., 2015; H.-S. Park et al., 2015; Woods & Caballero, 2016; Gong et al., 2017; B. Luo et al., 2017; Zhong et al., 2018; Chen et al., 2018; Graham, Itkin, et al., 2019). The increased frequency of these events has been linked to recent winter surface warming and sea ice loss in reanalyses (e.g., Woods & Caballero, 2016). Potential drivers of the increased frequency include increased tropical convection in the Pacific warm pool (Baggett & Lee, 2017) and increased Ural blocking (D. Luo et al., 2016; Gong & Luo, 2017; Chen et al., 2018; B. Luo et al., 2019; Tyrlis et al., 2019; Dai & Deng, 2022).

Cardinale and Rose (2022) defined an *efficiency* metric for the surface impact of synoptic-scale F_{trop} events, measuring the fraction of excess available energy per event that heats the surface, as opposed to being lost upward across the tropopause. This metric was applied to the recent historical period using the Modern-Era Retrospective analysis for Research and Applications, Version 2 (MERRA-2; GMAO, 2015). Efficiency was shown to vary widely, but composite analysis revealed two key determining factors: the vertical structure of F_{trop} and the preconditioning of the Arctic surface. High-efficiency events are associated with both lower pre-existing sea ice concentration (SIC) and more bottom-heavy F_{trop} anomalies. Reduced SIC results in reduced lower-tropospheric stability (LTS) and increased turbulent mixing—increasing the coupling between the surface and troposphere and enhancing downward turbulent heat flux anomalies (Cardinale & Rose, 2022). Furthermore, the frequency of high-efficiency events increased in MERRA-2 at the expense of low-efficiency events between 1980 and 2020, indicating an increase in the winter-mean efficiency. A potential driver of this increased efficiency is a decrease in Arctic LTS, suggesting a positive feedback loop.

The specific goal of this work is to apply the event-based efficiency metric from Cardinale and Rose (2022) to an ensemble of climate model simulations in order to assess systematic changes in Arctic winter-season surface heating in response to greenhouse gas forcing. We use simulations from the Community Earth System Model Large Ensemble (CESM-LE; Kay et al., 2015) with a strong radiative forcing scenario (RCP8.5). CESM-LE exhibits a relatively large Arctic amplification (Holland & Landrum, 2021), and thus is expected to exhibit a decrease in F_{wall} (Boeke & Taylor, 2018). Our key questions here include: (1) What are the forced changes in winter-season F_{wall} and F_{trop} in the warming climate? (2) Does the efficiency of F_{trop} events increase? (3) What is the net change in winter-season surface heating, accounting for changes in both F_{trop} and its efficiency? We hypothesize that an increase in the efficiency mitigates the decrease in F_{trop} in the CESM-LE.

2 Poleward energy flux and its changes in the CESM-LE

2.1 Datasets and methods

The CESM-LE includes a 40-member ensemble with a strong radiative forcing scenario to isolate the forced response to greenhouse gases. We compare data from the historical simulations (years 1990–2005; referred to as 20C) with RCP8.5 simulations for years 2071–80. These year ranges are selected based on availability of the necessary three-dimensional, high-frequency model output. We compute energy fluxes (F_{wall}, F_{trop}) directly following Cardinale et al. (2021), using 6-hourly instantaneous data at 70°N (meridional winds, atmospheric temperature, specific humidity, and geopotential height). Prior to the calculation of energy fluxes, we interpolate the 30 hybrid sigma-pressure levels to 28 pressure levels from 1000 to 5 hPa; the interpolated output in the troposphere has a vertical resolution of 25 hPa below 700 hPa, 50 hPa between 500 and 700 hPa, and a 100 hPa resolution above 500 hPa. To assess model bias, we compare the 20C ensemble to MERRA-2 from 1980 to 2020.

Before computing efficiency (see below), we must first account for the energy required to warm and moisten the Arctic troposphere. We define the Net Tropospheric Energy Source (NTES) as:

$$\text{NTES} = F_{\text{trop}} - \int_{300}^{P_s} \langle \frac{\partial h_{\text{m}}}{\partial t} \rangle \frac{dp}{g}, \tag{1}$$

where h_{m} is the moist enthalpy, and angle brackets indicate area-averages over the polar cap (70–90°N in this study). NTES represents the maximum energy available for surface heating following a surge in F_{trop}. The h_{m} tendency term is near zero in the winter mean, but is important on synoptic time scales (Cardinale & Rose, 2022).

2.2 Winter mean climatology in the 20C ensemble

Winter (NDJFM) mean polar cap–averaged temperature profiles and energy flux convergence metrics in 20C are shown in Figures 1a and 1b. The climatological winter mean 20C temperature profile is characterized by a surface inversion from 1000 to 850 hPa (Figure 1a). In the winter mean, F_{wall} supplies 116 W m^{-2} to the Arctic (Figure 1b). The vertical structure of F_{wall} in 20C is qualitatively similar to MERRA-2 (Cardinale et al., 2021); F_{wall} is bimodal, with local maxima in the troposphere at the top of the stable boundary layer and in the stratosphere (not shown). The winter mean F_{trop} is smaller than F_{wall}, supplying 95 W m^{-2}, with LH convergence contributing 13.5 W m^{-2} or 14%. At this seasonal scale, NTES and F_{trop} are very similar due to the small seasonal moist enthalpy tendencies.

2.3 Comparison between the 20C ensemble and MERRA-2

Winter mean atmospheric temperatures are generally similar to MERRA-2 except in the upper troposphere and stratosphere (Figure 1a; cf. blue and black lines). The surface inversion is also stronger in the CESM-LE. The stronger surface inversion is consistent with the overestimated stability over Arctic sea ice in CMIP5 models compared to reanalyses (Pithan et al., 2014), which has been linked to the shortcomings in the representation of mixed-phase clouds.

All terms in Figure 1b are overestimated by 2–6 W m^{-2} compared to MERRA-2, which lies outside the ensemble range (cf. blue vertical lines and white circles). Note that the MERRA-2 terms are averaged between 1980 and 2020; these differences are slightly reduced when the 1990–2005 period is used (not shown).

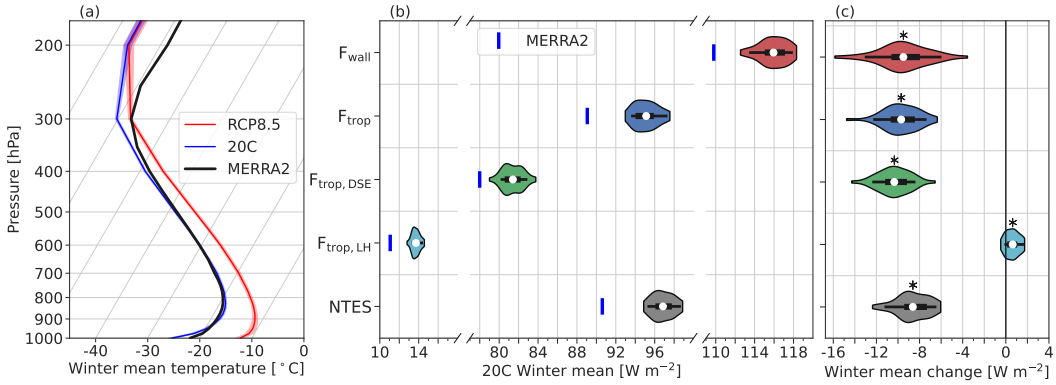

Figure 1. (a) Winter (NDJFM) mean polar cap–averaged (70–90°N) temperature profiles in 20C (1990–2005; blue) and RCP8.5 (2071–2080; red), compared to MERRA-2 (1980–2020; black); shading indicates the ensemble 5th–95th percentile range. (b) Winter mean total vertically integrated polar cap–averaged moist static energy (MSE) flux convergence (F_{wall}; red; $\mathrm{W\,m^{-2}}$), the tropospheric contribution to F_{wall} (F_{trop}; blue; $\mathrm{W\,m^{-2}}$), contributions to F_{trop} from the dry static energy (DSE; green; $\mathrm{W\,m^{-2}}$) and latent heat (LH; cyan; $\mathrm{W\,m^{-2}}$), and the net tropospheric energy source (NTES; gray; $\mathrm{W\,m^{-2}}$) in 20C runs, compared to MERRA-2 (blue vertical lines). (c) Winter-mean change from 20C to RCP8.5. Ensemble distributions are illustrated with violin plots, where shading indicates the probability density, thin horizontal lines indicate the 5th–95th percentile range, thick horizontal lines indicate the interquartile range, and white circles indicate the mean. Asterisks in (c) indicate ensemble means significantly different from 0 at the 95% confidence level.

2.4 Changes in energy flux convergence in the RCP8.5 scenario

Concurrent with a surface amplified warming and weaker surface inversion (Figure 1a), winter mean F_{wall} and F_{trop} both decrease in RCP8.5 by about 9.5 $\mathrm{W\,m^{-2}}$ (Figure 1c). A decrease in F_{wall} is consistent with the relatively large winter Arctic amplification factor of approximately 3 (Boeke & Taylor, 2018). The ensemble-mean changes in F_{trop} and F_{wall} are nearly identical, but the ensemble spread in F_{trop} changes are smaller compared to F_{wall}. An increase in the LH component appears to only partially compensate the decrease in DSE. NTES decreases by about 8.5 $\mathrm{W\,m^{-2}}$ and has a smaller ensemble spread than both F_{wall} and F_{trop}. All terms in Figure 1c are significantly different from 0. A traditional top-of-atmosphere budget attribution (e.g., Hahn et al., 2021) would thus infer that changes in atmospheric energy flux contribute to Arctic surface cooling (a mitigating factor for Arctic amplification).

3 The surface heating efficiency of F_{trop} events

3.1 The efficiency metric

We now define the efficiency E_{trop} following Cardinale and Rose (2022):

$$E_{\text{trop}} = \frac{\langle \mathrm{NSF}' \rangle}{\mathrm{NTES}'}, \tag{2}$$

where NSF is the net *downward* surface flux (the sum of turbulent energy fluxes and net longwave radiation), and primes indicate anomalies relative to the daily mean annual cycle. These anomalies are computed separately for each ensemble member and time period (20C and RCP8.5) and are linearly detrended to ensure stationary time series. Only

10–15 years are available for each simulation, so a smoothing low-pass filter with a cut-off frequency of 12 days is applied to each term before calculating the mean annual cycle. During periods where F_{trop} is anomalously large and the likely dominant driver of anomalous surface fluxes, E_{trop} approximates the fraction of the anomalous atmospheric source that heats the Arctic surface.

The mean annual cycle of NSF (see supplemental Figure S1) is not driven by F_{trop} events. Rather, the seasonality is best explained by the absorbed solar radiation during summer (large increase and decrease in dashed lines between April and November in Figure S1a) and sea ice growth during winter, which acts to suppress upward turbulent heat fluxes (increase in blue and red lines from November to April in Figure S1c). Thus, the winter mean E_{trop}, calculated with anomalies relative to the daily mean annual cycle, measures the coupling between F_{trop} and the NSF and approximates the fraction of the raw NTES that reaches the surface. The partial contribution to the time mean NSF from the atmosphere can be approximated as:

$$\langle\overline{\text{NSF}_{\text{atm}}}\rangle = \overline{E_{\text{trop}}}\ \overline{\text{NTES}}, \tag{3}$$

where overbars indicate the winter mean. While E_{trop} in Equation 3 is still calculated with anomalies relative to the daily mean annual cycle, it approximates the total (i.e., raw) atmospheric source that heats the surface in the winter mean. Note that in computing $\overline{E_{\text{trop}}}$, we neglect periods where E_{trop} is greater than 1 or less than 0 (about 40% of days); these are periods where NTES anomalies are generally small and have little potential to drive anomalous surface heating (not shown, but see Cardinale & Rose, 2022).

Another interpretation of $\overline{E_{\text{trop}}}$ is the slope of the regression line between NSF and NTES (Figure S2). These slopes in the 20C simulations (blue lines) are all close to 50%, remarkably similar to the ensemble mean $\overline{E_{\text{trop}}}$ calculated from Equation 2 (see Figure 4a).

3.2 Efficiency-based composites of F_{trop} events

Following Cardinale and Rose (2022), we define events based on a cumulative increase in NTES′ of 8 MJ m^{-2} (which gives a reasonable synoptic separation between events). There are 60.5±4.5 events per decade in the 20C ensemble mean. Events are then separated into three bins based on event-mean efficiency: high ($E_{\text{trop}} \geq 0.63$, the 75th percentile), low ($E_{\text{trop}} \leq 0.44$, the 25th percentile), and medium. Thus, high-efficiency events are those for which roughly two-thirds of NTES′ goes into surface heating. Percentile thresholds are similar to those in MERRA-2 (Cardinale & Rose, 2022).

To understand the processes determining E_{trop} in the CESM-LE, we compare composites of the anomalous tropospheric energy budget and lower-tropospheric stability (LTS; calculated as the potential temperature difference between 850 hPa and 2-m) in high, medium, and low-efficiency events (Figure 2) in 20C. Composites of the vertical structure of the time-integrated anomalous MSE and LH flux convergence in the 14 days before the central date of an event is shown in Figures 2a–c. High and medium-efficiency events are associated with bottom-heavy F_{trop} anomalies that are significantly different from low-efficiency events.

We assess Arctic preconditioning using the mean LTS between days −21 and −7 (Figures 2d–f). High-efficiency events occur in the presence of significantly lower LTS than for medium or low-efficiency events. This suggests a greater coupling between the atmosphere and surface during high-efficiency events, resulting in enhanced near-surface warming and moistening due to increased vertical mixing. Another interpretation of the differences between high and medium-efficiency comes from a Lagrangian prospective: as anomalously warm and moist air propagates through a stably stratified Arctic, it ascends along or slightly less than the slope of isentropic surfaces (Komatsu et al., 2018; You et al., 2021). In high-efficiency events, the reduced LTS allows for the warm and moist air to remain closer to the surface.

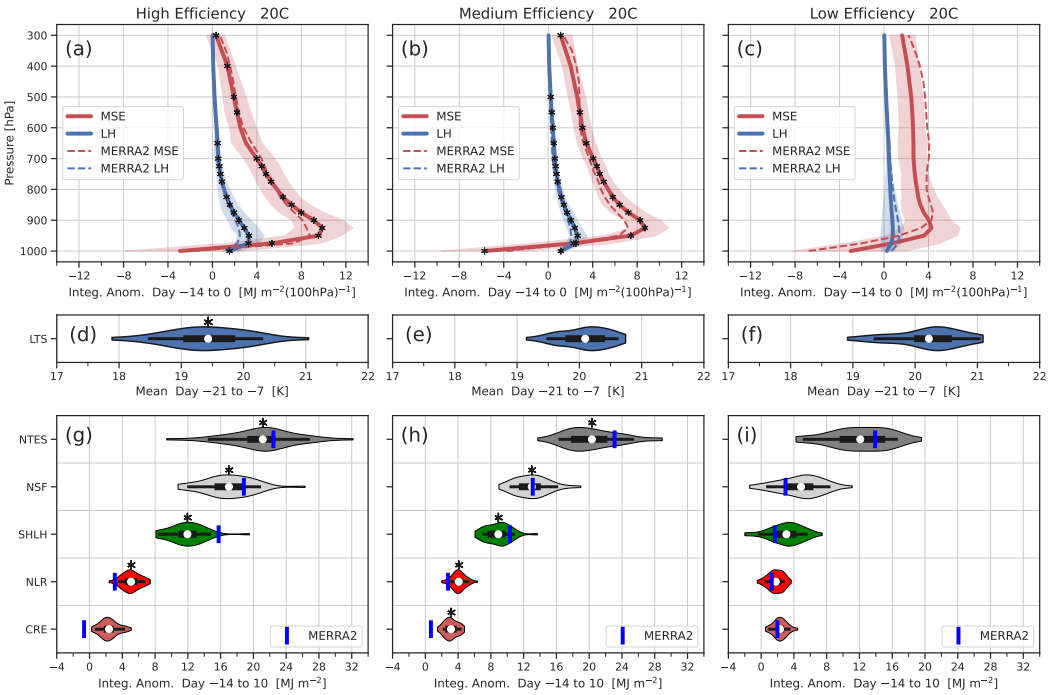

Figure 2. (a)–(c) Composite time-integrated anomalous MSE (red) and LH (blue) flux convergence from day −14 to 0 in 20C (solid) compared to MERRA-2 (dashed). (d)–(f) Mean LTS between days −21 and −7 in 20C. (g)–(h) Time-integrated anomalies in net tropospheric energy source (NTES), net surface flux (NSF), combined sensible and latent turbulent heat fluxes (SHLH), net longwave radiation (NLR), and surface cloud radiative effect (CRE) from day −14 to −10 in 20C, compared to MERRA-2. Violin plots follow the same convention as in Figure 1. Shading in (a)–(c) indicates the ensemble 5th–95th percentile range. Asterisks indicate ensemble means statistically different from low-efficiency events at 95% confidence

Differences in the Arctic preconditioning can be explained by the seasonality of events. High-efficiency events mainly occur in early winter when sea ice concentration (SIC) and associated LTS is relatively low, while medium and low-efficiency events mainly occur in mid-winter (Figure S3a). The association between stability and SIC is consistent with Deser et al. (2010) and Vihma (2014) and is closely related to turbulent heat fluxes.

Time-integrated anomalies in the tropospheric energy budget between days −14 and 10 are shown in Figures 2g–i. While both the net longwave radiation (NLR) and turbulent heat flux (SHLH) anomalies in high and medium-efficiency anomalies are significantly different from low-efficiency events, differences in E_{trop} are best explained by SHLH. Downward SHLH anomalies account for about 77% of the increase in E_{trop} from low to high-efficiency events during this period (cf. green violin plots between composites). Surface cloud radiative effect (CRE; NLR−$\text{NLR}_{\text{clear-sky}}$) anomalies are small but positive in all three composites, consistent with Johansson et al. (2017) and Liu et al. (2018), who found that cloud amounts increase during these episodic events.

3.3 Event composite comparison between MERRA-2 and 20C

The vertical structure of the MSE and LH flux convergence anomalies in 20C is similar to MERRA-2 (dashed and solid lines in Figures 2a–c). Tropospheric energy budget terms in MERRA-2 (blue vertical lines in Figures 2g–i) lie within the ensemble range,

except for the surface CRE anomalies in high and medium-efficiency events (Figures 2g and 2h). CRE differences between the CESM-LE and MERRA-2 potentially result from errors in the parameterization of cloud physics in MERRA-2 (Graham, Cohen, et al., 2019) or from a larger LTS prior to events in the CESM-LE.

The smaller increase in SHLH anomalies from low to high efficiency in the CESM-LE potentially results from the smaller upward SHLH during winter in the CESM-LE (Figure S1); i.e., less potential for suppressed SHLH during events. The larger increase in NLR anomalies from low to high efficiency in the CESM-LE potentially results from a larger increase in anomalous LH flux convergence and a smaller decrease in anomalous CRE from low to high efficiency.

There are about 10 fewer F_{trop} events per decade in the ensemble mean, compared to the MERRA-2 (not shown). This result is consistent with the negative moist intrusion density bias in the Atlantic sector (Woods et al., 2017); which is the hot spot for F_{trop} events (Cardinale & Rose, 2022).

3.4 Changes in event frequency and mean efficiency

Having validated the methodology of Cardinale and Rose (2022) applied to 20C, we now use the RCP8.5 ensemble to investigate forced changes in efficiency under a warming climate. We calculate E_{trop} for 2071–2080 using Equation 2 with anomalies relative to the new, warmer annual cycle. Figure 3 shows changes in relative frequency of high, medium, and low-efficiency events between 20C and RCP8.5. High-efficiency events increase, while medium and low-efficiency events decrease in frequency in the majority of members. All ensemble mean differences are significant. The high-efficiency event increase of 13.4 events per decade—mainly during the early to midwinter (Figure S3c)—is nearly compensated by a decrease in medium- and (especially) low-efficiency events. Consistently, we find that winter-mean $\overline{E_{\text{trop}}}$ increases from 50.2 to 55.9% in RCP8.5 (Figure 4a).

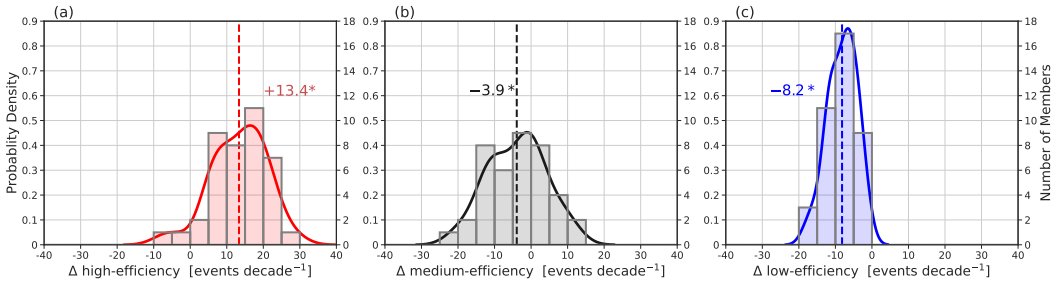

Figure 3. Winter mean change in frequency of (a) high (red), (b) medium (black), and (c) low-efficiency (blue) events per decade between 20C and RCP8.5. Ensemble means shown as dashed vertical lines, with asterisks indicating significant differences from 0 at 95% confidence.

We speculate that the increase in efficiency from 20C to RCP8.5 results from decreasing LTS associated with sea ice loss. Figure S4 shows that SHLH is the dominant term in the increased downward NSF′, which is plausibly a consequence of decreased LTS and greater coupling between the surface and troposphere. LH flux convergence and longwave radiation appears to play secondary roles. Note that despite a large increase in winter clouds (not shown, but consistent with decreased LTS, e.g., Taylor et al., 2015), the contribution from the surface CRE decreases in the RCP8.5 ensemble mean. A potential explanation for this is that cloud fractions are already high at the start of an event.

3.5 The implications of increasing efficiency

The change in the contribution to the time mean NSF from the atmosphere can be written as:

$$\Delta\langle\overline{\mathrm{NSF_{atm}}}\rangle = \Delta(\overline{E_{\mathrm{trop}}}\ \overline{\mathrm{NTES}}) \approx \overline{E_{\mathrm{trop}}}\ \Delta(\overline{\mathrm{NTES}}) + \Delta(\overline{E_{\mathrm{trop}}})\ \overline{\mathrm{NTES}}, \tag{4}$$

where the uppercase delta indicates the winter mean change and where we have invoked a linear approximation on the right-hand side (RHS). As in Hahn et al. (2021), the partial surface temperature change can be attributed by dividing the negative change in each term on the RHS of Equation 4 by the Planck feedback. Here, we use the local Arctic Planck feedback factor (approximately $-2.7\ \mathrm{W\,m^{-2}\,K^{-1}}$; Zhang et al., 2020). This attribution method provides only an approximate value for the partial surface temperature change, as it assumes that each term results in a vertically uniform warming.

Figure 4b shows the contribution from NTES and E_{trop} changes to the NSF (i.e., the surface energy budget). The first term of Equation 4 on the RHS (blue histogram) indicates that a decrease in the NTES contributes to surface cooling (approximately 1.6 K), reducing the NSF by 4.3 $\mathrm{W\,m^{-2}}$. The second term of Equation 4 on the RHS (black histogram) indicates that an increase in E_{trop} contributes to surface warming (approximately 2 K), increasing the NSF by 5.5 $\mathrm{W\,m^{-2}}$.

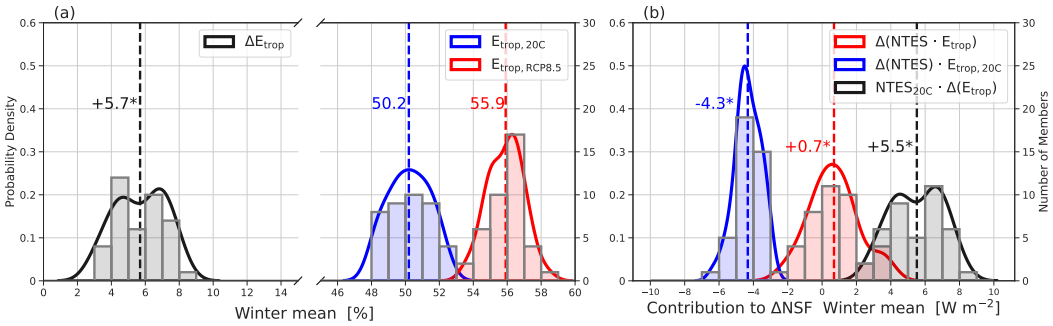

Figure 4. (a) Winter mean surface heating efficiency ($\overline{E_{\mathrm{trop}}}$) in 20C (blue) and RCP8.5 (red) and the difference (black). (b) Contribution to the winter mean change in NSF from changes in $\overline{\mathrm{NTES}}$ ($\overline{E_{\mathrm{trop}}}$ fixed at 20C values; blue), changes in $\overline{E_{\mathrm{trop}}}$ ($\overline{\mathrm{NTES}}$ fixed at 20C values; black), and the combined change (red). Asterisks indicate ensemble mean changes significantly different from 0 at 95% confidence.

The increase in E_{trop} compensates the decrease in F_{trop} (red histogram in Figure 4b). A small, but statistically significant, increase in the energy gained by the surface (0.7 $\mathrm{W\,m^{-2}}$ or approximately 0.3 K of surface warming) results from a larger contribution from the change in E_{trop}, with about 65% of members agreeing on the sign of the change.

4 Conclusions

In this study, we investigated the role of atmospheric circulations on Arctic (70–90°N) warming during the winter (NDJFM) in the RCP8.5 warming scenario of the CESM large ensemble. We argued that changes in the polar cap–averaged tropospheric energy flux convergence (F_{trop}) and changes in the coupling between F_{trop} and the surface energy budget should be considered when quantifying the contribution from atmospheric energy transport to Arctic surface warming. The coupling can be measured by the surface heating efficiency (E_{trop}), which approximates the fraction of an anomalous F_{trop} that goes into anomalous surface heating after accounting for tropospheric heating and

moistening. Importantly, when calculating E_{trop}, synoptic variability must be taken into account.

Winter mean F_{trop} was found to decrease by 9.5 W m^{-2} from 20C to RCP8.5, dominated by decreased dry static energy and only partially compensated by latent heat. Winter mean E_{trop} was found to increase by 5.7% (from 50.2 to 55.9%). Importantly, only days with an E_{trop} between 0 and 1 were used to calculate winter means, which eliminates periods where the atmosphere is not the dominant driver of NSF anomalies. The increase in E_{trop} can also be visualized by the steeper slope of the regression of NSF on NTES in RCP8.5 simulations (cf. blue and red lines in Figure S2).

Composite analysis of high, medium, and low-efficiency events reveal that E_{trop} is largest during events with reduced lower-tropospheric stability (LTS) and bottom-heavy F_{trop}, confirming key findings of Cardinale and Rose (2022). Consistent with the increase in the winter mean E_{trop}, the frequency of high-efficiency events was found to increase by 13.4 events per decade. Results suggest that the increase in efficiency is a response to decreasing sea ice and associated reduction in LTS, which enhances the coupling between the surface and troposphere.

The net effect of the decrease in F_{trop} and increase in E_{trop} is a small positive contribution to Arctic surface warming during winter. This result supports the hypothesis that an increase in E_{trop} mitigates the decrease in F_{trop} and prevents the damping of Arctic amplification in the CESM-LE.

The use of the large ensemble allows us to interpret the efficiency increase as a forced response to greenhouse gases. It is also important to consider the robustness of these results to inter-model differences, particularly as the sign of the change of F_{wall} is inconsistent across models (Hwang et al., 2011; Boeke & Taylor, 2018). Because our results suggest that E_{trop} increases primarily due to loss of stratification, we expect that E_{trop} will increase robustly with Arctic warming (and thus contribute to enhanced surface warming) independently of changes in F_{trop}. The mitigation that we have found in CESM-LE may be a model-specific result, but efficiency very likely increases in most models under future warming scenarios.

5 Open Research

MERRA-2 data are available through the Goddard Earth Sciences (GES) Data and Information Services Center (DISC) archive (GMAO, 2015). CESM-LE data are available through the Amazon Web Services Simple Storage Service (AWS S3; de La Beaujardière et al., 2019). Calculations and analysis with CESM-LE data were performed using Pangeo Cloud, a cloud-based research platform (Abernathey et al., 2021). The code to reproduce the results will be made available at `https://github.com/cjcardinale/Cardinale-Rose-2022-GRL`.

Acknowledgments

CJC and BEJR were supported by NSF grant ICER-2026863.

References

Abernathey, R. P., Augspurger, T., Banihirwe, A., Blackmon-Luca, C. C., Crone, T. J., Gentemann, C. L., ... Signell, R. P. (2021). Cloud-native repositories for big scientific data. *Computing in Science Engineering*, *23*(2), 26-35. doi: 10.1109/MCSE.2021.3059437

Baggett, C., & Lee, S. (2017). An Identification of the Mechanisms that Lead to Arctic Warming During Planetary-Scale and Synoptic-Scale Wave Life Cycles.

J. Atmos. Sci., *74*(6), 1859-1877. doi: 10.1175/JAS-D-16-0156.1

Boeke, R. C., & Taylor, P. C. (2018). Seasonal energy exchange in sea ice retreat regions contributes to differences in projected arctic warming. *Nature communications*, *9*(1), 5017–5017. doi: 10.1038/s41467-018-07061-9

Cardinale, C. J., & Rose, B. E. J. (2022). The arctic surface heating efficiency of tropospheric energy flux events. *J. Climate*, 1 - 39. (published online ahead of print) doi: 10.1175/JCLI-D-21-0852.1

Cardinale, C. J., Rose, B. E. J., Lang, A. L., & Donohoe, A. (2021). Stratospheric and tropospheric flux contributions to the polar cap energy budgets. *Journal of Climate*, *34*(11), 4261 - 4278. doi: 10.1175/JCLI-D-20-0722.1

Chen, X., Luo, D., Feldstein, S. B., & Lee, S. (2018). Impact of winter ural blocking on arctic sea ice: Short-time variability. *J. Climate*, *31*(6), 2267 - 2282. doi: 10.1175/JCLI-D-17-0194.1

Cohen, J., Screen, J., Furtado, J., Barlow, M., Whittleston, D., Coumou, D., ... Jones, J. (2014). Recent arctic amplification and extreme mid-latitude weather. *Nature Geoscience*, *7*, 627-637. doi: 10.1038/ngeo2234

Dai, A., & Deng, J. (2022). Recent eurasian winter cooling partly caused by internal multidecadal variability amplified by arctic sea ice-air interactions. *Climate Dyn.*. doi: 10.1007/s00382-021-06095-y

de La Beaujardière, J., Banihirwe, A., Shih, C. F. G., Paul, K., & Hamman, J. (2019). *Ncar cesm lens cloud-optimized subset.* UCAR/NCAR Computational and Information Systems Lab. doi: 10.26024/wt24-5j82

Deser, C., Tomas, R., Alexander, M., & Lawrence, D. (2010). The seasonal atmospheric response to projected arctic sea ice loss in the late twenty-first century. *Journal of Climate*, *23*(2), 333 - 351. doi: 10.1175/2009JCLI3053.1

GMAO. (2015). *MERRA-2 inst3_3d_asm_Np: 3d,3-Hourly,Instantaneous,Pressure-Level,Assimilation,Assimilated Meteorological Fields V5.12.4.* Greenbelt, MD, USA: Goddard Earth Sciences Data and Information Services Center (GES DISC). (Accessed November 2020) doi: 10.5067/QBZ6MG944HW0

Doyle, J. G., Lesins, G., Thackray, C. P., Perro, C., Nott, G. J., Duck, T. J., ... Drummond, J. R. (2011). Water vapor intrusions into the high arctic during winter. *Geophysical Research Letters*, *38*(12). doi: https://doi.org/10.1029/2011GL047493

Feldl, N., Po-Chedley, S., Singh, H. K. A., Hay, S., & Kushner, P. J. (2020). Sea ice and atmospheric circulation shape the high-latitude lapse rate feedback. *npj Climate and Atmospheric Science*, *3*(1), 41. doi: 10.1038/s41612-020-00146-7

Gong, T., Feldstein, S., & Lee, S. (2017). The role of downward infrared radiation in the recent arctic winter warming trend. *J. Climate*, *30*. doi: 10.1175/JCLI-D-16-0180.1

Gong, T., & Luo, D. (2017). Ural blocking as an amplifier of the arctic sea ice decline in winter. *Journal of Climate*, *30*(7), 2639 - 2654. doi: 10.1175/JCLI-D-16-0548.1

Goosse, H., Kay, J. E., Armour, K. C., Bodas-Salcedo, A., Chepfer, H., Docquier, D., ... Vancoppenolle, M. (2018). Quantifying climate feedbacks in polar regions. *Nature Communications*, *9*(1), 1919. doi: 10.1038/s41467-018-04173-0

Graham, R. M., Cohen, L., Ritzhaupt, N., Segger, B., Graversen, R. G., Rinke, A., ... Hudson, S. R. (2019). Evaluation of six atmospheric reanalyses over arctic sea ice from winter to early summer. *Journal of Climate*, *32*(14), 4121 - 4143. doi: 10.1175/JCLI-D-18-0643.1

Graham, R. M., Itkin, P., Meyer, A., Sundfjord, A., Spreen, G., Smedsrud, L. H., ... Granskog, M. A. (2019). Winter storms accelerate the demise of sea ice in the Atlantic sector of the Arctic Ocean. *Sci Rep*, *9*(1), 9222. doi: 10.1038/s41598-019-45574-5

Graversen, R. G., & Burtu, M. (2016). Arctic amplification enhanced by latent energy transport of atmospheric planetary waves. *Q.J.R. Meteorol. Soc*,

142(698), 2046-2054. doi: 10.1002/qj.2802

Graversen, R. G., & Langen, P. L. (2019). On the role of the atmospheric energy transport in 2 × co2–induced polar amplification in cesm1. *J. Climate*, *32*(13), 3941 - 3956. doi: 10.1175/JCLI-D-18-0546.1

Hahn, L. C., Armour, K. C., Zelinka, M. D., Bitz, C. M., & Donohoe, A. (2021). Contributions to polar amplification in cmip5 and cmip6 models. *Frontiers in Earth Science*, *9*. doi: 10.3389/feart.2021.710036

Henry, M., Merlis, T. M., Lutsko, N. J., & Rose, B. E. J. (2021). Decomposing the drivers of polar amplification with a single column model. *J. Climate*, *34*, 2355–2365. doi: 10.1175/JCLI-D-20-0178.1

Holland, M. M., & Landrum, L. (2021). The emergence and transient nature of arctic amplification in coupled climate models. *Frontiers in Earth Science*, *9*. doi: 10.3389/feart.2021.719024

Hwang, Y.-T., Frierson, D. M. W., & Kay, J. E. (2011). Coupling between arctic feedbacks and changes in poleward energy transport. *Geophysical Research Letters*, *38*(17). doi: https://doi.org/10.1029/2011GL048546

Johansson, E., Devasthale, A., Tjernström, M., Ekman, A. M. L., & L'Ecuyer, T. (2017). Response of the lower troposphere to moisture intrusions into the arctic. *Geophysical Research Letters*, *44*(5), 2527-2536. doi: https://doi.org/10.1002/2017GL072687

Kay, J. E., Deser, C., Phillips, A., Mai, A., Hannay, C., Strand, G., ... Vertenstein, M. (2015). The community earth system model (cesm) large ensemble project: A community resource for studying climate change in the presence of internal climate variability. *Bulletin of the American Meteorological Society*, *96*(8), 1333 - 1349. doi: 10.1175/BAMS-D-13-00255.1

Koenigk, T., Brodeau, L., Graversen, R. G., Karlsson, J., Svensson, G., Tjernström, M., ... Wyser, K. (2013). Arctic climate change in 21st century cmip5 simulations with ec-earth. *Climate Dyn.*, *40*(11), 2719–2743. doi: 10.1007/s00382-012-1505-y

Komatsu, K. K., Alexeev, V. A., Repina, I. A., & Tachibana, Y. (2018). Poleward upgliding siberian atmospheric rivers over sea ice heat up arctic upper air. *Scientific Reports*, *8*(1), 2872. doi: 10.1038/s41598-018-21159-6

Liu, Y., Key, J. R., Vavrus, S., & Woods, C. (2018). Time evolution of the cloud response to moisture intrusions into the arctic during winter. *Journal of Climate*, *31*(22), 9389 - 9405. doi: 10.1175/JCLI-D-17-0896.1

Luo, B., Luo, D., Wu, L., Zhong, L., & Simmonds, I. (2017). Atmospheric circulation patterns which promote winter arctic sea ice decline. *Environmental Research Letters*, *12*(5), 054017. doi: 10.1088/1748-9326/aa69d0

Luo, B., Wu, L., Luo, D., Dai, A., & Simmonds, I. (2019). The winter midlatitude-arctic interaction: effects of north atlantic sst and high-latitude blocking on arctic sea ice and eurasian cooling. *Climate Dyn.*, *52*(5), 2981–3004. doi: 10.1007/s00382-018-4301-5

Luo, D., Xiao, Y., Yao, Y., Dai, A., Simmonds, I., & Franzke, C. L. E. (2016). Impact of ural blocking on winter warm arctic–cold eurasian anomalies. part i: Blocking-induced amplification. *Journal of Climate*, *29*(11), 3925 - 3947. doi: 10.1175/JCLI-D-15-0611.1

D.-S. R. Park, Lee, S., & Feldstein, S. B. (2015). Attribution of the Recent Winter Sea Ice Decline over the Atlantic Sector of the Arctic Ocean. *J. Climate*, *28*(10), 4027-4033. doi: 10.1175/JCLI-D-15-0042.1

H.-S. Park, Lee, S., Son, S.-W., Feldstein, S. B., & Kosaka, Y. (2015). The Impact of Poleward Moisture and Sensible Heat Flux on Arctic Winter Sea Ice Variability. *J. Climate*, *28*(13), 5030-5040. doi: 10.1175/JCLI-D-15-0074.1

Pithan, F., & Mauritsen, T. (2014). Arctic amplification dominated by temperature feedbacks in contemporary climate models. *Nature Geoscience*, *7*(3), 181–184. doi: 10.1038/ngeo2071

Pithan, F., Medeiros, B., & Mauritsen, T. (2014). Mixed-phase clouds cause climate model biases in arctic wintertime temperature inversions. *Climate Dyn.*, *43*(1), 289–303. doi: 10.1007/s00382-013-1964-9

Screen, J. A., & Simmonds, I. (2010). The central role of diminishing sea ice in recent arctic temperature amplification. *Nature*, *464*(7293), 1334-1337. doi: https://doi.org/10.1038/nature09051

Taylor, P. C., Boeke, R. C., Boisvert, L. N., Feldl, N., Henry, M., Huang, Y., ... Tan, I. (2022). Process drivers, inter-model spread, and the path forward: A review of amplified arctic warming. *Frontiers in Earth Science*, *9*. doi: 10.3389/feart.2021.758361

Taylor, P. C., Kato, S., Xu, K.-M., & Cai, M. (2015). Covariance between arctic sea ice and clouds within atmospheric state regimes at the satellite footprint level. *Journal of Geophysical Research: Atmospheres*, *120*(24), 12656-12678. doi: https://doi.org/10.1002/2015JD023520

Tyrlis, E., Manzini, E., Bader, J., Ukita, J., Nakamura, H., & Matei, D. (2019). Ural blocking driving extreme arctic sea ice loss, cold eurasia, and stratospheric vortex weakening in autumn and early winter 2016–2017. *Journal of Geophysical Research: Atmospheres*, *124*(21), 11313-11329. doi: https://doi.org/10.1029/2019JD031085

Vihma, T. (2014). Effects of arctic sea ice decline on weather and climate: A review. *Surveys in Geophysics*, *35*(5), 1175–1214. doi: 10.1007/s10712-014-9284-0

Woods, C., & Caballero, R. (2016). The Role of Moist Intrusions in Winter Arctic Warming and Sea Ice Decline. *J. Climate*, *29*(12), 4473-4485. doi: 10.1175/JCLI-D-15-0773.1

Woods, C., Caballero, R., & Svensson, G. (2013). Large-scale circulation associated with moisture intrusions into the arctic during winter. *Geophysical Research Letters*, *40*(17), 4717-4721. doi: https://doi.org/10.1002/grl.50912

Woods, C., Caballero, R., & Svensson, G. (2017). Representation of arctic moist intrusions in cmip5 models and implications for winter climate biases. *J. Climate*, *30*(11), 4083 - 4102. doi: 10.1175/JCLI-D-16-0710.1

You, C., Tjernström, M., & Devasthale, A. (2021). Warm-air advection over melting sea-ice: A lagrangian case study. *Boundary-Layer Meteorology*, *179*(1), 99–116. doi: 10.1007/s10546-020-00590-1

Zhang, R., Wang, H., Fu, Q., & Rasch, P. J. (2020). Assessing global and local radiative feedbacks based on agcm simulations for 1980–2014/2017. *Geophysical Research Letters*, *47*(12), e2020GL088063. doi: https://doi.org/10.1029/2020GL088063

Zhong, L., Hua, L., & Luo, D. (2018). Local and external moisture sources for the arctic warming over the barents–kara seas. *Journal of Climate*, *31*(5), 1963 - 1982. doi: 10.1175/JCLI-D-17-0203.1

Supporting Information for "The Increasing Efficiency of the Poleward Energy Transport into the Arctic in a Warming Climate"

Christopher J. Cardinale[1], and Brian E. J. Rose[1]

[1]Department of Atmospheric and Environmental Sciences, University at Albany, State University of New York, Albany, New York

Contents of this file

1. Figures S1 to S4

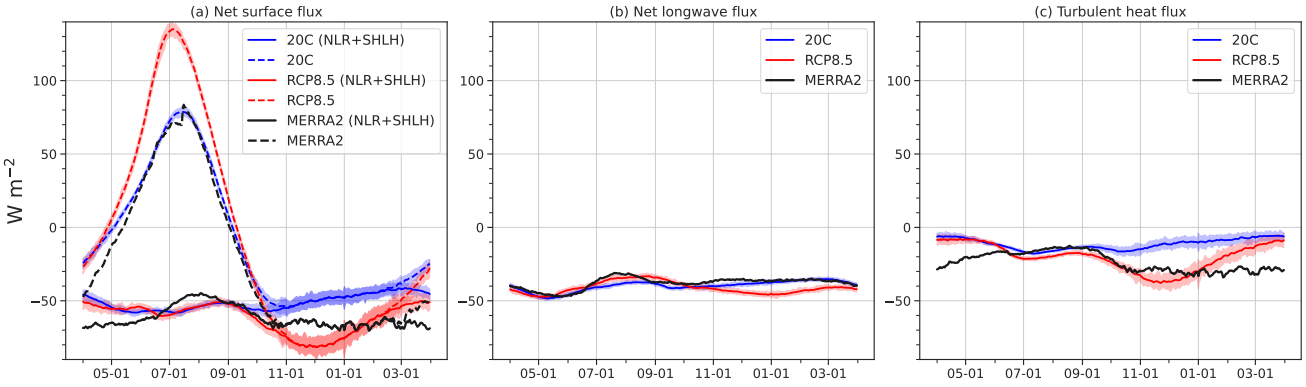

Figure S1. Mean annual cycle of the polar cap–averaged (a) net surface flux (NSF; dashed; including net absorbed shortwave radiation) and contributions to the NSF from the combined net longwave and turbulent heat fluxes (NLR+SHLH; solid; not including shortwave radiation), (b) net longwave flux, and (c) turbulent heat fluxes (SHLH). All panels are positive down (atmosphere to surface) in units of W m^{-2}, and comparing the 20C (blue) and RCP8.5 (red) simulations from the CESM-LE to the MERRA-2 (black). Shading indicates the ensemble 5th–95th percentile range.

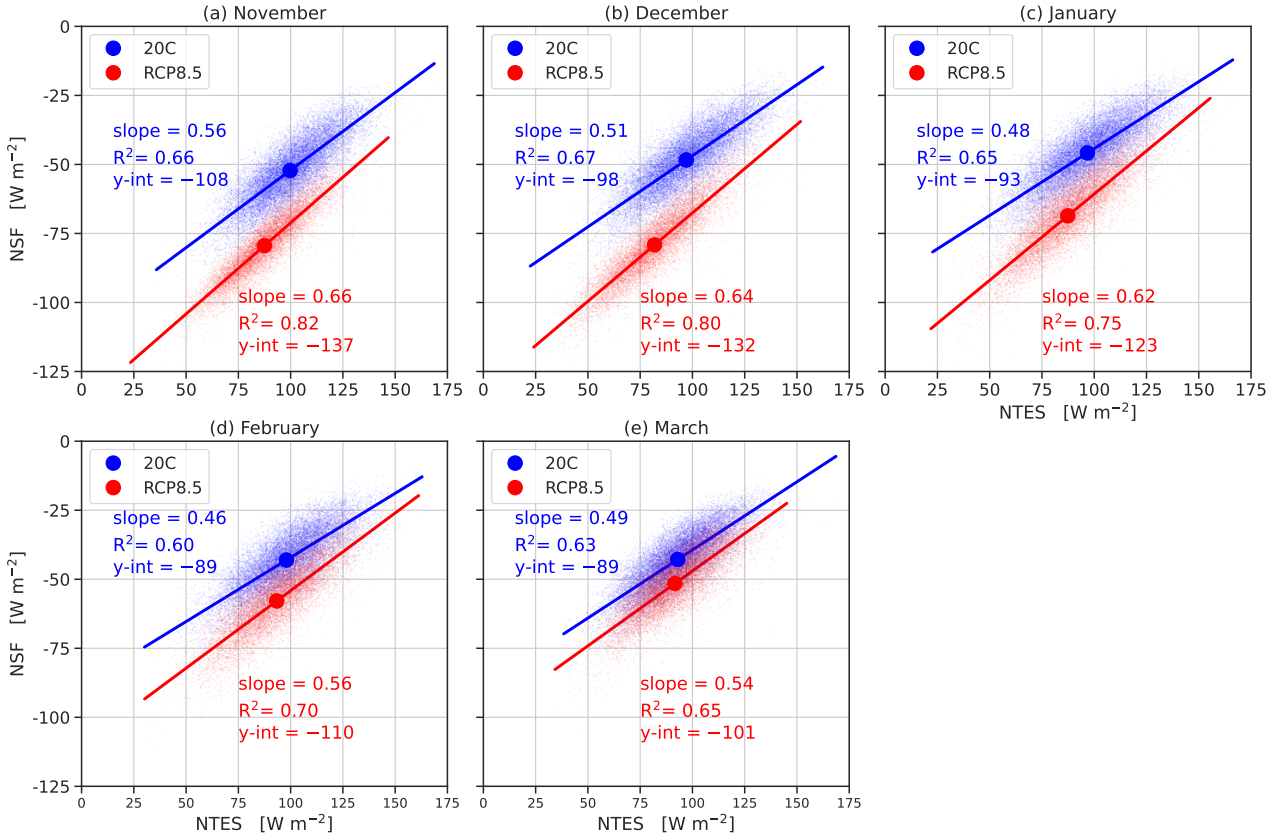

Figure S2. Daily mean NSF against NTES during (a)–(e) each winter month (November–March) in the 20C (blue; $\mathrm{W\,m^{-2}}$) and RCP8.5 (red; $\mathrm{W\,m^{-2}}$) runs of the CESM-LE. For each ensemble and month, the linear regression (solid lines), climatological mean (large circles), slope, coefficient of determination ($\mathrm{R^2}$), and y-intercept ($\mathrm{W\,m^{-2}}$) are shown. Grouping by month reduces the impact of the seasonal cycle on the slopes of the regression lines.

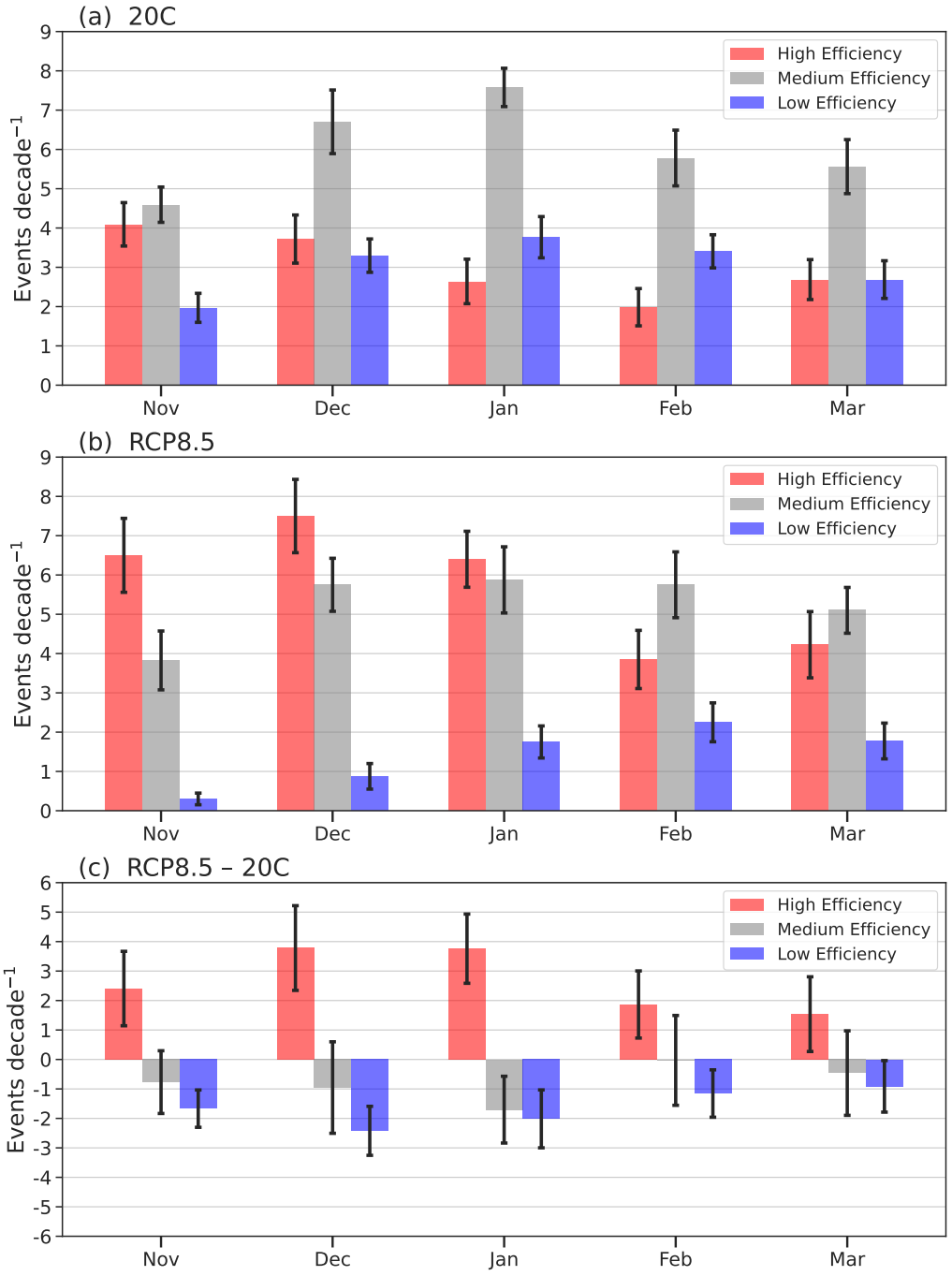

Figure S3. Average number of high (red), medium (gray), and low-efficiency (blue) events per decade for each winter month in the (a) 20C and (b) RCP8.5 runs of the CESM-LE. (c) shows the difference (RCP8.5 – 20C). Vertical lines indicate the 95% confidence interval.

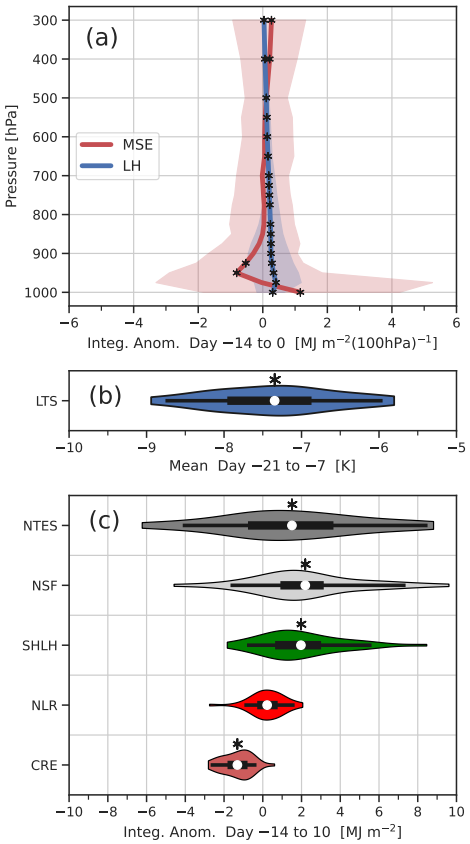

Figure S4. Composite of the change (RCP8.5 − 20C) in the (a) time-integrated anomalous local moist static energy (MSE; red) and latent heat (LH; blue) flux convergence [MJ m^{-2} (100 hPa)$^{-1}$] from day −14 to 0 in F_{trop} events (combined high, medium, and low-efficiency events). (b) shows the change in mean lower-tropospheric stability (LTS; blue; K) between days −21 and −7. (c) shows the change in time-integrated anomalies in the net tropospheric energy source (NTES; gray; MJ m^{-2}), net surface flux (NSF; light gray; MJ m^{-2}), combined sensible and latent surface turbulent heat fluxes (SHLH; green, MJ m^{-2}), net longwave radiation (red; MJ m^{-2}), and surface cloud radiative effect (CRE; MJ m^{-2}) from day −14 to −10. Violin plots follow the same convention as in Fig. 1. The shading in (a) indicates the ensemble 5th–95th percentile range. Asterisks indicate ensemble means statistically different from low-efficiency events at 95% confidence.